Sustainable Food Technology

ROYAL SOCIETY OF CHEMISTRY

PAPER

View Article Online
View Journal

Cite this: DOI: 10.1039/d5fb00753d

Biodegradable alginate–sericin biofilm: a colorimetric indicator using mangosteen-peel anthocyanins for protein food freshness

Thi-Hong-No Nguyen, [ab] Minh-Truong Truong,[c] Minh-Ty Nguyen,[a] Quynh-Nhu Pham, [a] Dinh-Tri Mai,[ab] Thi-Quynh-Nhu Ngo,[a] Thi-Ngoc-Mai Tran,[d] Ngoc-Bich-Tuyen Nguyen,[d] Chi-Hien Dang, [ab] Huu-Trung Nguyen,[e] Cao-Hien Nguyen[f] and Thanh-Danh Nguyen *[ab]

Smart indicator films provide an eco-friendly approach for real-time monitoring of food freshness through easily interpretable visual color changes. In this work, a fully biodegradable pH-responsive film was fabricated from sodium alginate and silk sericin (SS), with anthocyanins extracted from discarded mangosteen peel (ASA) serving as the natural chromatic indicator. Structural analyses verified the formation of a stable Alg–SS network that enhanced swelling resistance, lowered solubility, and improved moisture-barrier properties. Among all formulations, the film containing 7% anthocyanin (ASA7) exhibited the most favorable balance of functional attributes, including a strong and stable colorimetric response, adequate mechanical strength, and moderate hydrophilicity. The ASA7 film also demonstrated pronounced antioxidant activity, with scavenging efficiencies of 37.10 ± 1.71% (DPPH) and 90.37 ± 1.30% (H_2O_2). Distinct, reversible color transitions from pink-red to blue occurred as pH increased, enabling reliable visual sensing. When applied to pork and shrimp packaging, the film's color evolution showed strong correlation with total volatile basic nitrogen (TVB-N), accurately signaling the spoilage threshold (25 mg N/100 g). Overall, the ASA film presents a promising waste-derived indicator system for intelligent food packaging, offering real-time freshness assessment while supporting sustainability and circular-economy goals.

Received 28th October 2025
Accepted 7th January 2026

DOI: 10.1039/d5fb00753d

rsc.li/susfoodtech

Sustainability spotlight

This work stems from our ongoing research on sustainable polysaccharide-based biomaterials and their applications in intelligent food packaging and freshness biosensing. We developed a novel biodegradable, pH-responsive smart film composed of sodium alginate, silk sericin and anthocyanins extracted from waste mangosteen peel, a valorized agro-industrial by-product. The integration of these waste-derived materials generated a compact and functional biopolymer matrix with enhanced barrier performance, antioxidant capacity, and colorimetric response. The optimized ASA film exhibited distinct and reversible color transitions correlated with total volatile basic nitrogen (TVB-N) accumulation during shrimp and pork spoilage, enabling real-time, non-destructive freshness monitoring.

1 Introduction

Driven by increasing environmental awareness and stringent food safety regulations, smart biodegradable films have emerged as a promising class of next-generation packaging materials. These intelligent systems integrate responsive and sensing functionalities, enabling real-time monitoring of food freshness and quality throughout storage and distribution. Smart biofilms represent a new generation of food packaging systems that not only protect and preserve products but also actively monitor freshness and detect spoilage through measurable visual changes. By integrating natural sensing components, these films provide real-time indicators of food quality, thereby enhancing consumer confidence and reducing food waste.[1,2]

[a]Institute of Advanced Technology, Vietnam Academy of Science and Technology, 01B TL29, An Phu Dong Ward, Ho Chi Minh City, 700000, Vietnam. E-mail: danh5463bd@yahoo.com
[b]Graduate University of Science and Technology, Vietnam Academy of Science and Technology, 18 Hoang Quoc Viet, Cau Giay District, Hanoi, Vietnam
[c]Ton Duc Thang University, 19 Nguyen Huu Tho, Ho Chi Minh City, Vietnam
[d]Institute of Applied Sciences, HUTECH University, 475A Dien Bien Phu Street, Thanh My Tay Ward, Ho Chi Minh City, Vietnam
[e]Faculty of Chemical Engineering, Industrial University of Ho Chi Minh City, 12 Nguyen Van Bao, Ho Chi Minh City, Vietnam
[f]Department of Chemical Technology, Ho Chi Minh City University of Industry and Trade, Ho Chi Minh City 700000, Vietnam

Among natural functional colorants, anthocyanins are particularly attractive for intelligent packaging applications due to their water solubility, antioxidant and antimicrobial activities, and pronounced pH-dependent color transitions, which allow them to act as reliable freshness indicators.[3,4] Recent research trends have moved toward nano-encapsulation and multi-component integration to optimize pigment stability and sensing performance. For instance, Shiryanpour *et al.* (2025) reported nanoemulsion-based active films incorporating anthocyanin-loaded systems for poultry preservation, demonstrating extended shelf-life and enhanced pigment stability.[5] Similarly, Choubaki *et al.* (2025) developed a nanoencapsulated anthocyanin composite film capable of detecting fish spoilage through clear chromatic transitions,[6] while Xu Chen *et al.* (2025) highlighted an improved stable and multifunctional intelligent film based on grape skin anthocyanin, polyvinyl alcohol, chitosan and selenopeptide.[7] These emerging approaches reflect the shift towards hybrid active-intelligent systems, where pigments simultaneously function as preservatives and indicators.

Waste mangosteen (*Garcinia mangostana*) peel, an abundant agro-industrial by-product accounting for approximately 60–65% of the total fruit weight, represents an underexploited source rich in anthocyanins (14–20%).[8] Valorizing this discarded biomass not only contributes to circular economy goals but also provides a low-cost and eco-friendly route for producing pH-responsive colorimetric indicators.

Sericin (SS), a natural protein derived from *Bombyx mori* silk cocoons, constitutes approximately 20–30% of the total cocoon protein and acts as an adhesive coating that binds fibroin fibers together.[9] During the degumming step of silk processing, SS is commonly removed and discarded in the wastewater stream, generating a large amount of protein-rich effluent that contributes to environmental pollution in silk-producing regions such as Vietnam. The valorization of this industrial by-product therefore represents an eco-friendly strategy that supports waste minimization and circular bioeconomy objectives.[10,11] Chemically, SS is rich in polar amino acids such as serine, aspartic acid, and glycine, which provide abundant hydroxyl (–OH), carboxyl (–COOH), and amino ($–NH_2$) groups capable of forming hydrogen bonds and electrostatic interactions with polysaccharides.[10] These functional groups facilitate the formation of stable interpolymeric networks when combined with natural polysaccharides such as alginate, chitosan, or pectin, resulting in enhanced mechanical strength, flexibility, and moisture resistance.[12,13] Moreover, SS is biodegradable and biocompatible, as it can be enzymatically degraded by proteases, and inherently possesses antioxidant, antibacterial, UV-protective, and moisture-retaining properties, which make it an attractive functional component for active and intelligent food-packaging systems.[10,12] Recent developments have demonstrated that SS-based or SS-reinforced biopolymer films can effectively improve film transparency, structural integrity, and bioactivity while maintaining full biodegradability.[14] Consequently, the incorporation of SS, a waste-derived silk protein with natural biofunctionality, into polysaccharide matrices provides a sustainable and high-value approach for designing eco-friendly smart films capable of freshness monitoring and active food preservation.

Sodium alginate (Alg) is a natural anionic polysaccharide extracted primarily from brown seaweeds such as *Laminaria* and *Macrocystis*, and is widely recognized for its excellent film-forming ability, biodegradability, non-toxicity, and biocompatibility.[15,16] Structurally, alginate consists of linear copolymers of β-D-mannuronic acid (M) and α-L-guluronic acid (G) residues, which allow the formation of ionic crosslinks with divalent cations (*e.g.*, Ca^{2+}), generating three-dimensional "egg-box" networks with enhanced flexibility, mechanical strength, and stability in biopolymer matrices.[17] When combined with proteins such as SS, alginate promotes strong interpolymeric hydrogen bonding and electrostatic interactions, improving matrix integrity and elasticity, which makes it a highly compatible support for pH-responsive indicators like anthocyanins. Such hybrid systems are particularly advantageous in smart films designed for monitoring the freshness of protein-based foods such as seafood and meat, where the total volatile basic nitrogen (TVB-N) compounds, mainly ammonia, dimethylamine, and trimethylamine, accumulate during spoilage and induce measurable pH shifts.[18,19] These pH variations lead to distinct color changes in anthocyanin-incorporated smart films, enabling consumers and retailers to visually assess product freshness without the need for destructive testing. Due to these combined functional, optical, and sensing properties, alginate-based smart films have attracted increasing attention in recent years. Current research trends emphasize bio-based intelligent films integrating alginate with other natural polysaccharides, such as chitosan, gelatin, and pectin, and plant-derived colorants (anthocyanins) for freshness monitoring of highly perishable foods including shrimp, meat, and fish.[20–24]

To the best of our knowledge, this study is the first to incorporate anthocyanins extracted from discarded mangosteen peel into a dual-component Alg/SS matrix, creating a multifunctional biodegradable film that simultaneously exhibits active biofunctionality and intelligent colorimetric sensing. The synergistic integration of SS with alginate strengthens the polymer network, enhances structural stability, and improves barrier performance, while the pigment-rich mangosteen peel extract provides both antioxidant activity and a highly sensitive pH-responsive chromatic shift. Unlike most existing indicator systems that are restricted to a single food type, the developed film demonstrates reliable freshness sensing for both shrimp and red meat, two matrices characterized by distinct spoilage mechanisms, highlighting its broad-spectrum applicability and practical relevance. This work therefore encompasses the valorization of mangosteen peel waste through pigment extraction and characterization, the fabrication and optimization of ASA composite films, comprehensive assessment of their physicochemical, mechanical, barrier, and optical properties, and validation of their pH-dependent color transitions for real-time monitoring of seafood and red-meat freshness.

2 Materials and methods

2.1. Materials

Silk cocoons of *B. mori* were sourced from Bao Loc, Vietnam. Mangosteen peels were obtained from Tan Phat Ho Chi Minh Co., Vietnam, and dried to a moisture content of less than 10%. Triton X-100 and DPPH (99.55%) were supplied by Sigma-Aldrich. Sodium alginate was supplied by Himedia, India. Hydrochloric acid (37.0%), sodium hydroxide (98.0%), sodium chloride (99.0%), potassium chloride (98.0%), anhydrous sodium carbonate (98.0%), potassium dihydrogen orthophosphate, anhydrous disodium hydrogen orthophosphate (98.0%), glacial acetic acid (99.5%), and ethanol (99.0%) were obtained from Fisher. Meat and shrimp samples were purchased from a local supermarket in District 12, Ho Chi Minh City, Vietnam, between January and May, 2025.

2.2. Sericin extraction

Silk sericin (SS) was extracted from *B. mori* cocoons according to the method reported in ref. 25 with slight modifications. Briefly, 50 g of silk cocoons were cut into small fragments and immersed in deionized water (1 : 10 w/v). The suspension was autoclaved at 125 °C for 120 min to hydrothermally separate SS from fibroin fibers. After cooling, the mixture was filtered to remove the insoluble fibroin, and the obtained SS solution was freeze-dried to yield a fine, light-yellow powder. The dried SS powder was stored in amber bottles at 8 °C until further use. The extraction process provided a yield of 19.17 ± 0.02%, with a protein content of 79–82%, consistent with previous reports for hydrothermally derived sericin.

2.3. Anthocyanin extraction

Anthocyanins (ACs) were extracted from waste mangosteen (*G. mangostana*) peels following a previously reported procedure with slight modifications.[8] Fresh peels were thoroughly washed, oven-dried, and ground into a fine powder. The extraction was carried out using a 2% (w/v) citric acid solution as the solvent, at a solid-to-liquid ratio of 1 : 5 (w/v). The mixture was subjected to ultrasound-assisted extraction in an ultrasonic bath for 45 min to facilitate pigment release. After sonication, the suspension was filtered through fine filter cloth to remove coarse residues, followed by centrifugation to collect the supernatant. The obtained extract was subsequently freeze-dried to yield powdered AC. The dried AC powder was stored in sealed, light-resistant containers at 5–10 °C to minimize degradation and moisture uptake. The yield of crude anthocyanin extracted powder was determined by the gravimetric method, using the following eqn (1)

$$\text{Anthocyanin extraction yield}(\%) = \frac{\text{weight of dried anthocyanin powder}}{\text{weight of dried sample}} \times 100 \quad (1)$$

The total anthocyanin content was quantified following the general principles reported by Hiranrangsee *et al.* (2016),[26] with appropriate modifications to suit the current study. Briefly, 0.01 g of crude anthocyanin extracted powder was dispersed in a 10 mL volumetric flask and made up to volume using 0.025 M potassium chloride buffer (pH 1.0). A second aliquot was prepared similarly using 0.4 M sodium acetate buffer (pH 4.5). Both solutions were left to equilibrate for 30 minutes at ambient temperature, after which absorbance was recorded at 510 and 700 nm.

Anthocyanin concentration was calculated using eqn (2)

$$\text{Total anthocyanin content}\left(\text{mg g}^{-1}\right) = \frac{A \times M_W \times D_F \times 10^{-3}}{\varepsilon \times l \times m} \quad (2)$$

where the absorbance difference (A) was calculated as:

$$A = (A_{510} - A_{700})_{\text{pH1.0}} - (A_{510} - A_{700})_{\text{pH4.5}}$$

M_W represents the molecular weight of cyanidin-3-glucoside (449.2 g mol^{-1}), D_F is the dilution factor, ε is the molar extinction coefficient (26 900 L mol^{-1} cm^{-1}), l is the path length of the cuvette (1 cm), and m is the crude anthocyanin extracted powder (0.01 g).

The peel extract exhibited an anthocyanin yield of 17.8 ± 0.3% w/w (based on dried peel), with a quantified concentration of 173.9 ± 1.4 mg per g cyanidin-3-glucoside equivalents per anthocyanin extract powder.

2.4. Fabrication of alginate/sericin/anthocyanin (ASA) composite films

The alginate/sericin/anthocyanin (ASA) composite films were prepared following the procedure described by Nguyen *et al.*,[25] with minor modifications. In brief, a 2% (w/v) sodium alginate solution was mixed with a 1% (w/v) SS solution and stirred continuously at 70 °C for 2 h to ensure complete homogenization of the biopolymer matrix. Glycerol was incorporated as a plasticizer at a constant level of 30% (w/w) relative to the total polymer content to improve the flexibility and reduce brittleness of the films. Subsequently, anthocyanin extract obtained from mangosteen peels was added to the film-forming solution at concentrations of 0, 5, 7, 10, and 12% (v/v) to evaluate its effect on the colorimetric sensitivity and antioxidant properties of the resulting films. The homogeneous mixtures were cast into Petri dishes and dried at 50 °C for 24 h in a hot-air oven. The dried films were carefully peeled off and conditioned in a desiccator for 24 h at room temperature prior to physicochemical characterization and functional analysis. The optimized film was prepared using 2% (w/v) alginate, 1% (w/v) sericin, and 7% (v/v) anthocyanin, based on preliminary screening experiments aimed at achieving good film integrity, mechanical strength, and a stable color change response.

2.5. Physicochemical characterization

2.5.1. Swelling ratio and water solubility. The swelling ratio of the film was determined following a previously reported method with minor modifications.[22] Film samples were cut into square pieces (20.0 mm × 20.0 mm) and their initial mass was recorded. The samples were then exposed to ambient conditions to allow natural swelling. After reaching equilibrium, the

swollen films were weighed, and the swelling ratio was calculated using eqn (3):

$$\text{Swelling ratio}(\%) = \frac{m_1 - m_0}{m_0} \times 100\% \quad (3)$$

where m_0 (g) represents the initial mass of the film before swelling and m_1 (g) is the mass after swelling.

The water solubility of the film was evaluated based on a previously established method with slight modifications.[27] Briefly, Alg/SS-based films with varying anthocyanin concentrations were dried in an oven at 105 °C for 24 hours. The dried films were then cut into pieces (3–5 cm) and weighed to determine their initial dry mass. Each sample was immersed in 30 mL of distilled water and incubated at room temperature for 24 hours. After incubation, the films were removed, re-dried at 105 °C for another 24 hours, and weighed again. The water solubility was then calculated using eqn (4):

$$\text{Water solubility}(\%) = \frac{m_0 - m_2}{m_0} \times 100\% \quad (4)$$

where m_0 (g) is the initial dry mass of the film and m_2 (g) represents the final mass of the film after the drying process.

2.5.2. Water vapor permeability. The water vapor permeability (WVP) of the film was determined following a previously reported method with modifications,[28] with reference to ASTM E96. This experiment aimed to evaluate the ability of the ASA film to inhibit water vapor transmission. In brief, a test tube containing 10 g of dry silica gel was sealed with the film and placed in a desiccator filled with distilled water. The tube was maintained at a constant temperature of 32 °C. The weight of the test tube was recorded every 24 hours until a constant value was reached. The WVP of each film was calculated using eqn (5):

$$\text{WVP}\left(\text{g m}^{-1}\ \text{s}^{-1}\ \text{Pa}^{-1}\right) = \frac{w \times x}{A \times t \times (P_2 - P_1)} \quad (5)$$

where w is the weight loss of the test tube (g) over time t (s), x is the thickness of the tested film (m), A is the exposed surface area of the film (m^2), and ($P_2 - P_1$) represents the water vapor pressure difference across the film (Pa).

2.5.3. The light-blocking properties. The light-blocking properties of the film were assessed using a UV-vis spectrophotometer, following the previous method.[29,30] The rectangular film samples (2 × 3 cm) were analyzed with an infrared absorption spectrophotometer (UV-vis/NIR), model V-770 (Jascos, Japan). Spectral scans were performed over the wavelength range of 200 to 800 nm. Film opacity was subsequently determined using the following formula (6):

$$\text{Opacity} = \frac{\text{Abs } 600}{x} \quad (6)$$

where Abs 600 is the absorbance of the film at a wavelength of 600 nm, and x: corresponds to the film thickness. The UV-barrier efficiency of the films was determined based on light transmittance (%).

2.5.4. Mechanical properties. The mechanical properties of the films were determined following a previously reported method[31] with reference to ASTM D882-18 for thin plastic films. Tensile strength (TS) and elongation at break (EB) of the ASA film were measured at 25 °C using a Multitest 5-xt apparatus (Mecmesin, UK). Film strips (30 mm × 80 mm) were prepared for testing. A crosshead speed of 100 mm min^{-1} was maintained during the measurements. TS (MPa) and EB (%) were calculated using eqn (7) and (8), respectively.

$$\text{TS(MPa)} = \frac{F_{\max}}{A} \quad (7)$$

$$\text{EB}(\%) = \frac{L}{30} \times 100 \quad (8)$$

where $F_{\max}$ is the maximum applied load (N) at film rupture, A is the cross-sectional area of the film (mm^2), and L is the elongation at rupture (mm).

2.5.5. Color measurement of films. Color analysis of the films with varying anthocyanin concentrations (ASA0, ASA5, ASA7, ASA10, and ASA12) was carried out to evaluate the effect of anthocyanin incorporation on the visual properties of the films. Each film sample was cut into 2 × 2 cm squares, and color parameters were determined using a colorimeter (CS-10 Colour Reader, CHN SPEC, China) based on the CIELAB color system. In this system, the lightness parameter (L^*) ranges from 0 (black) to 100 (white), representing brightness; the a^* coordinate indicates the green ($-a^*$) to red ($+a^*$) color axis, while the b^* coordinate represents the blue ($-b^*$) to yellow ($+b^*$) color axis. Variations in L^*, a^*, and b^* values reflect differences in anthocyanin concentration and distribution within the film matrix.[32]

2.5.6. Physicochemical measurements. The surface hydrophobicity of each film was determined using a MicroView USB Digital Microscope, equipped with Analysis Software (220 × 2.0 MP) for image processing. A drop of distilled water was carefully placed on the film surface, and the contact angle (θ) at the liquid–solid interface was measured. The measurements were carried out in triplicate.

To determine the presented functional groups, the films and their components were analyzed using a Bruker FTIR spectrophotometer (Japan) over a scanning range of 400–4000 cm^{-1}. The solid samples were measured in the presence of KBr.

Thermogravimetric analysis (TGA) was conducted using a Thermo plus TG 8120 and Differential Scanning Calorimetry (DSC) analysis of the film samples was conducted using a TA Instruments Discovery DSC 25 system (Waters L.L.C., USA). Thermal measurements were carried out over a temperature range of 40 to 400 °C. The heating rate was maintained at 10 °C per minute, while the nitrogen purge gas was supplied at a constant flow rate of 25 mL per minute.

2.6. Antioxidant activity

Antioxidant activity was expressed as percentage radical inhibition, as the objective of this analysis was to compare internal differences among film formulations.

2.6.1. DPPH method. The antioxidant activity of the films was assessed using the 2,2-diphenyl-1-picrylhydrazyl (DPPH) free radical assay, which measured the reduction of the stable DPPH radical exhibiting a characteristic absorption at 517 nm.[33] In brief, rectangular film specimens (1.0 cm^2) were immersed in

5.0 mL of an ethanolic 0.05 mM DPPH solution. The mixtures were gently stirred at room temperature for 30 min in the dark to avoid photodegradation of the radicals. After incubation, the absorbance at 517 nm was recorded using a UV-vis spectrophotometer, and the radical-scavenging activity was calculated relative to a negative control (ethanol solution without a film) processed under identical conditions. The radical scavenging activity (RSA) was calculated using eqn (9):

$$\mathrm{RSA}(\%) = \frac{A_0 - A_1}{A_0} \times 100 \quad (9)$$

where A_0 is the absorbance of the control and A_1 is the absorbance of the sample.

2.6.2. Hydrogen peroxide scavenging assay. The hydrogen peroxide scavenging (HPS) activity of the films was determined according to the procedure described by Mukhopadhyay *et al.* (2016),[34] with slight modifications. Briefly, 0.25 mL of ferrous ammonium sulfate (1.0 mM) was mixed with 1.5 mL of the film extract solution, followed by the addition of 62.5 μL of hydrogen peroxide (5.0 mM). The reaction mixture was incubated at room temperature for 5 min in the dark to prevent photodecomposition of hydrogen peroxide. Subsequently, 1.5 mL of 1,10-phenanthroline (1.0 mM) was added, and the mixture was thoroughly vortexed and allowed to stand for 10 min at room temperature. The formation of the orange-colored Fe^{2+}-phenanthroline complex was quantified by measuring the absorbance at 510 nm using a UV-vis spectrophotometer, and the HPS activity was expressed relative to the blank sample.

A blank solution containing 1.5 mL of 1,10-phenanthroline (1.0 mM), 1.56 mL of distilled water, and 0.25 mL of ferrous ammonium sulfate (1.0 mM) was prepared, and its highest absorbance value was used as a reference. The HPS value of the films was calculated using eqn (10).

$$\%\ \mathrm{HPS} = \frac{A_{\mathrm{sample}}}{A_{\mathrm{blank}}} \times 100 \quad (10)$$

2.7. Application and observation of films on shrimp and meat samples

The film application test was conducted by placing the films on fresh shrimp and meat samples to observe color changes and evaluate their potential as spoilage indicators during storage. The film was cut into 1.0 × 1.0 cm squares and used as colorimetric indicators. Each experimental setup consisted of shrimp/meat samples placed in an 11 cm diameter Petri dish, with the indicator film affixed to the inner surface of the lid. Fourteen experimental samples were prepared for each food type, namely shrimp and meat. All Petri dishes were stored at room temperature for observation. The evaluation included sensory indicators such as color, texture, smell, and taste (after boiling).

TVB-N values were determined *via* the Kjeldahl method[35] with slight modifications. Approximately 10 g of the sample are accurately weighed to within ±0.01 g and transferred directly into a distillation flask. Subsequently, around 3 g of magnesium oxide (MgO) and 100 mL of deionized water are added. The distillation flask is then set up within a distillation apparatus. A receiving flask containing 50 mL of boric acid solution is positioned to collect the distillate, ensuring that the outlet tube from the condenser is submerged in boric acid to effectively trap volatile bases. The distillation process is initiated and maintained for 15 minutes. Following distillation, the contents of the receiving flask are titrated with HCl solution (0.1 N) until the color shifts from green to grey. The total volatile basic nitrogen (TVB-N) content, expressed in mg of nitrogen per 100 grams of sample, is calculated using the following formula (11).

$$\mathrm{TVB\text{-}N}(\mathrm{mg\ N\ per\ 100\ g}) = \frac{V \times C \times 14.01 \times 100}{m} \quad (11)$$

where V is volume of HCl used in the titration (mL); C is concentration of HCl (N); m is mass of the sample (g); the value 14.01 is the molecular weight of nitrogen.

For colorimetric analysis, images of the biofilm samples were captured at 4 h intervals using a smartphone under consistent lighting conditions. The red–green–blue (RGB) color components were extracted using the online tool https://imagecolorpicker.com, and the obtained RGB values were subsequently processed to calculate the R/G, R/B, and G/B ratios. These ratios were plotted and statistically analyzed using OriginPro 2018 (OriginLab Corp., USA) to evaluate the temporal color variation of the films. To validate the observed colorimetric response, TVB-N was simultaneously determined and statistically correlated with the color change of the developed film.

3 Results and discussion

3.1. Fabrication of ASA biofilms

The present study was designed to address the dual objectives of valorizing agricultural byproducts and developing an environmentally friendly smart biofilm capable of visually monitoring food freshness in real time. The research strategy is illustrated in Fig. 1A. Protein SS contains high content of hydrophilic amino acids and reactive functional groups, which promote film formation and strong intermolecular interactions with alginate chains. This method may enhance mechanical strength and flexibility of alginate-based biofilms through the formation of ionic crosslinking. Anthocyanins extracted from waste mangosteen peel were utilized as natural colorimetric and antioxidant agents because of their pH-dependent color transitions and bioactive properties, which enable the film to respond sensitively to volatile nitrogen compounds released during the spoilage of protein-based foods.

By combining these three components, biodegradable ASA films were investigated to achieve optimal color stability, mechanical integrity, and antioxidant performance. The films were characterized in terms of their swelling behavior, water solubility, vapor permeability, light-blocking ability, and mechanical strength to understand the physicochemical factors governing their functionality. FTIR and DSC were applied to elucidate the intermolecular interactions and thermal stability within the polymer network, while antioxidant assays based on DPPH and HPS activity provided insights into their radical-neutralizing capability. The developed ASA films were subsequently applied to shrimp and meat samples to detect freshness

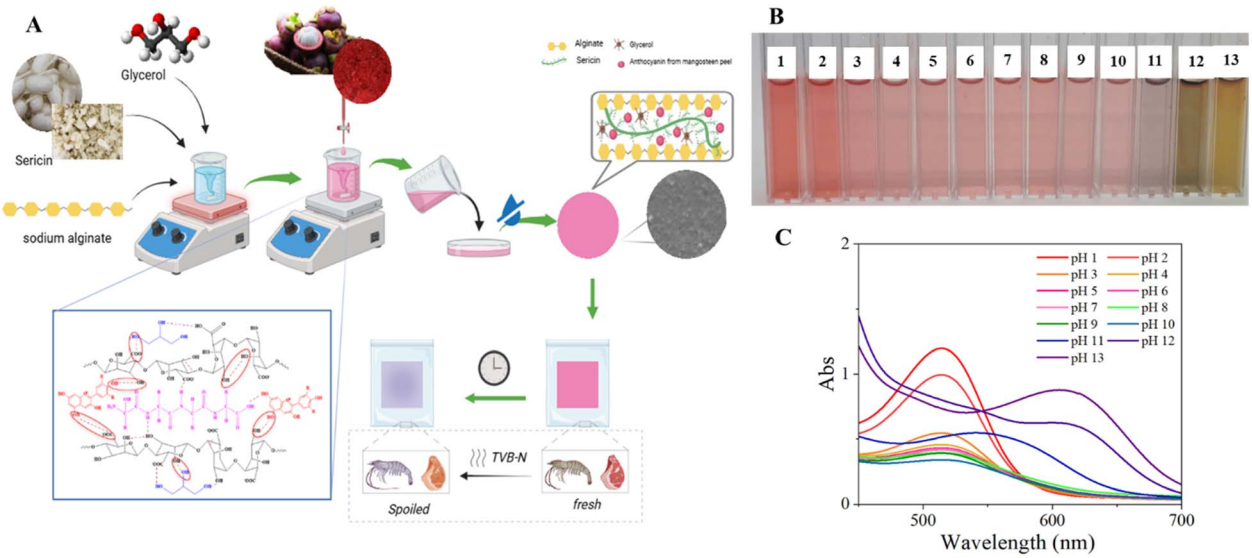

Fig. 1 The research strategy (A), color variations (B), and UV-vis spectra (C) of mangosteen anthocyanin solutions at different pH levels (1–13).

through visible color changes associated with TVB-N accumulation during storage. This systematic approach demonstrates an effective route to transform low-cost, natural residues into multifunctional smart films that combine biodegradability, sensory responsiveness, and potential for practical deployment in intelligent food-packaging systems.

Fig. 1B presents the visible color response of mangosteen-peel anthocyanin solutions across a wide pH range (1–13). The solutions displayed a distinct and gradual color transition from bright red under strongly acidic conditions (pH 1–3) to orange-red and violet tones in near-neutral environments (pH 5–9), eventually shifting to greenish-yellow at highly alkaline (pH 12–13). This chromatic progression reflects the pH-dependent structural equilibrium of anthocyanin molecules. At low pH, the dominant species is the flavylium cation, responsible for the intense red coloration. As the pH increases, the flavylium form undergoes hydration and tautomerization, yielding quinoidal bases and chalcone structures, which successively alter the absorption spectrum and produce bluish to greenish hues at higher pH values.[36] The pronounced green coloration observed at pH 12–13 corresponds primarily to the formation of deprotonated chalcone anions, consistent with previously reported anthocyanin transformations under alkaline conditions.[37] Similar pH-responsive color changes have also been documented in anthocyanin-based indicator films, confirming the suitability of these natural pigments for visual freshness sensing applications.[22]

The images and color parameters (L^*, a^*, b^*) of the alginate–sericin films containing various concentrations of mangosteen-peel anthocyanins are presented in Table 1. The incorporation of anthocyanins markedly influenced the optical appearance and chromatic attributes of the films. The L^* values, representing lightness, decreased progressively from 31.03 ± 1.23 in the anthocyanin-free film (ASA0) to 27.03 ± 1.05 for ASA5, 23.36 ± 1.74 for ASA7, 17.98 ± 0.39 for ASA10, and 13.67 ± 1.23 for ASA12. This steady reduction in brightness reflects the gradual darkening of the films as pigment concentration increased. The effect can be attributed to the strong absorption of visible light by anthocyanins, which intensify coloration and reduce transparency by scattering and absorbing incident light within the polymer matrix.

The a^* parameter, corresponding to the green–red color axis, exhibited a clear and consistent shift from negative to positive values with increasing anthocyanin content. The pure Alg/SS film (ASA0) displayed a greenish tone ($a^* = -6.85 \pm 2.46$), while the addition of anthocyanins transformed the color gradually to red: $a^* = 2.95 \pm 0.47$ (ASA5), 3.44 ± 0.24 (ASA7), 4.37 ± 0.38 (ASA10), reaching 15.87 ± 2.48 for ASA12. This continuous increase in a^* values confirms the successful incorporation, retention, and stability of anthocyanin molecules within the alginate–sericin matrix, where higher pigment concentrations amplify the red hue due to a greater proportion of flavylium ions dominating the visible absorption spectrum.

Meanwhile, the b^* coordinate, representing the blue–yellow axis, initially increased from 8.37 ± 0.09 (ASA0) to 17.03 ± 2.62 (ASA5), indicating a yellowish-red appearance at low pigment levels. Beyond this point, b^* values decreased gradually to 16.05 ± 0.92 (ASA7), 14.04 ± 0.37 (ASA10), and 8.84 ± 0.91 (ASA12), suggesting a visual shift from bright reddish-orange to deep purplish-red as the anthocyanin loading increased. This trend arises from overlapping absorption bands of the flavylium and quinoidal base forms of anthocyanins, which dominate under near-neutral to weakly acidic conditions.

These results demonstrate that anthocyanins derived from mangosteen peel not only impart strong coloration but also modulate the hue and saturation of the biopolymer films through concentration-dependent optical effects. Comparable findings were reported by Hamzah *et al.* (2022),[32] where starch films containing red-cabbage anthocyanins exhibited reduced L^* and enhanced a^* values, and by Yun *et al.* (2019),[38] who observed intensified red coloration in cassava starch films with Chinese bayberry extract. Consistent with these studies, the ASA

Table 1 The images and color parameters (L^*, a^*, b^*) of alginate–sericin–anthocyanin (ASA) composite films prepared with different mangosteen-peel anthocyanin concentrations[a]

	Color parameters		
Films	L^*	a^*	b^*
ASA0	31.03 ± 1.23^{e}	-6.85 ± 2.46^{a}	8.37 ± 0.09^{a}
ASA5	27.03 ± 1.05^{d}	2.95 ± 0.47^{b}	17.03 ± 2.62^{b}
ASA7	23.36 ± 1.74^{c}	3.44 ± 0.24^{b}	16.05 ± 0.92^{b}
ASA10	17.98 ± 0.39^{b}	4.37 ± 0.38^{b}	14.04 ± 0.37^{b}
ASA12	13.67 ± 1.23^{a}	15.87 ± 2.48^{c}	8.84 ± 0.91^{a}

[a] Data are presented as means ± standard deviation ($n = 3$). Values with different letters within the same row show significant differences ($p < 0.05$).

films became progressively darker and more reddish with increasing anthocyanin concentration, confirming the pigment's strong chromatic influence. The observed gradation in color parameters not only enhances the visual appeal of the films but also supports their potential as natural colorimetric indicators for detecting freshness-related pH shifts and volatile amine accumulation in perishable food products.

3.2. Effect of anthocyanin concentration on the physical and structural properties of ASA films

The effect of mangosteen-peel anthocyanin concentration on the physicochemical and mechanical properties of ASA films is summarized in Fig. 2. The swelling ratio, water solubility, and tensile behavior were found to be strongly dependent on the pigment content incorporated into the polymeric network. As shown in Fig. 2A, the swelling ratio decreased systematically with increasing anthocyanin concentration. The control film without pigment (ASA0) exhibited the highest water uptake of 16.8 ± 0.1%, indicating the high hydrophilicity and loose structure of the native Alg/SS matrix. Upon addition of 5% anthocyanin (ASA5), the swelling ratio declined sharply to 11.2 ± 0.2%, suggesting the onset of hydrogen-bond formation between anthocyanin hydroxyl groups and Alg/SS functional groups. Further increases in pigment content to 7%, 10%, and 12% led to successive reductions in swelling to 8.4 ± 0.1%, 6.1 ± 0.1%, and 5.3 ± 0.1%, respectively. This continuous suppression of water absorption indicates the progressive formation of a compact polymeric network, in which anthocyanins serve as multifunctional cross-linking agents bridging Alg/SS chains through non-covalent interactions. The resulting denser structure hindered water diffusion and retention within the matrix. Similar declining trends in swelling with polyphenol incorporation were observed by Luan Gustavo dos Santos *et al.*[39] in alginate–gellan gum films containing anthocyanins, corroborating the pivotal role of phenolic–polysaccharide hydrogen bonding in reducing hydrophilicity. In contrast, water solubility exhibited a gradual increase as anthocyanin loading increased, with the ASA12 film showing the highest solubility among all samples. This enhancement can be attributed to partial disruption of Alg/SS associations at high pigment levels, which reduced cohesive energy density and increased free volume within the network, allowing greater solvent penetration and dissolution of amorphous domains.

Leaching of anthocyanins is a key factor affecting the long-term stability of colorimetric films. In the ASA system, anthocyanins form hydrogen-bond and electrostatic interactions with Alg/SS functional groups, helping retain pigments despite their intrinsic water solubility. Swelling and solubility results show that higher pigment loading increases water solubility and thus the likelihood of leaching, consistent with earlier reports on alginate-based indicator films.[40] For the optimized ASA7 film, moderate hydrophilicity and low swelling (8.4 ± 0.1%) suggest sufficient pigment retention to maintain stable coloration during shrimp and pork storage tests. Only minimal leaching was observed under practical conditions, though slight pigment migration may occur during prolonged exposure in high-humidity environments.

The WVP value of ASA films (Fig. 2B) exhibited a consistent increase with higher anthocyanin concentrations, indicating that pigment incorporation affected both matrix density and hydrophilicity. At the initial stage, the WVP of the control film (ASA0) was $12.42 \pm 0.46 \times 10^{-10}$ g m^{-2} s^{-1} Pa^{-1}, and gradually increased to $15.40 \pm 0.13 \times 10^{-10}$ g m^{-2} s^{-1} Pa^{-1} for ASA5, $15.72 \pm 0.13 \times 10^{-10}$ g m^{-2} s^{-1} Pa^{-1} for ASA7, $14.94 \pm 0.11 \times 10^{-10}$ g m^{-2} s^{-1} Pa^{-1} for ASA10, and $14.69 \pm 0.34 \times 10^{-10}$ g m^{-2} s^{-1} Pa^{-1} for ASA12. A similar pattern persisted throughout the 8 h measurement period. After 8 h, the WVP values stabilized at $9.17 \pm 0.07 \times 10^{-10}$, $10.30 \pm 0.05 \times 10^{-10}$, 10.37 ± 0.08

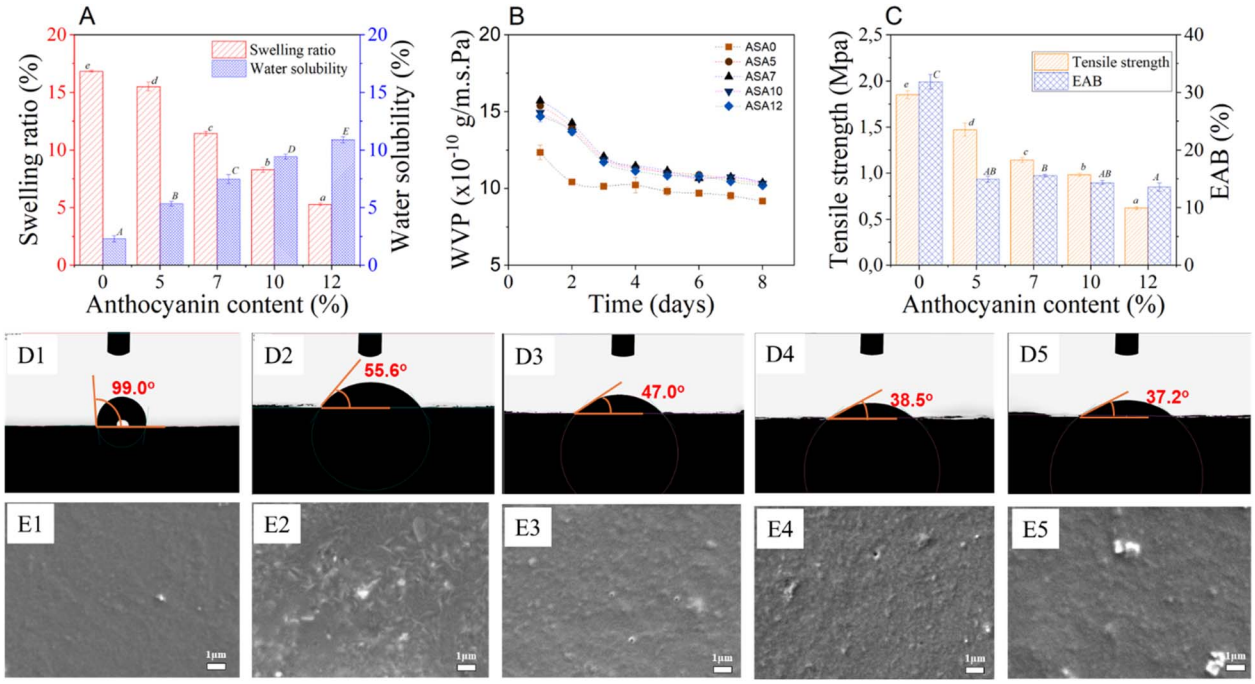

Fig. 2 Swelling ratio and water solubility (A); water vapor permeability (B); tensile strength and elongation at break intensity (C); contact angle images (D1–D5) and SEM micrographs (E1–E5) of the films at various anthocyanin contents: 0%, 5%,7%,10% and 12%.

$\times 10^{-10}$, $10.32 \pm 0.09 \times 10^{-10}$, and $10.17 \pm 0.11 \times 10^{-10}$ g m^{-2} s^{-1} Pa^{-1}, respectively. The overall WVP increase of approximately 15–20% from ASA0 to ASA7 reflects the influence of anthocyanin hydroxyl groups, which enhance water-vapor diffusion by increasing the number of polar sites within the network. At higher pigment levels (10–12%), the partial phase separation between hydrophilic anthocyanins and the Alg/SS backbone likely introduced micro-voids and discontinuities, providing additional pathways for vapor transmission.[41] Furthermore, the less compact polymer packing caused by pigment aggregation facilitated capillary-like vapor flow across the matrix. Nevertheless, the moderate decline in WVP at the highest pigment loading (ASA12) compared with ASA7 indicates that excessive anthocyanin may induce limited molecular rearrangement and partial collapse of the pore structure, resulting in slightly lower diffusivity. These results confirm that anthocyanins not only increase hydrophilicity but also alter the microstructure of the Alg–SS network, producing a more permeable yet structurally heterogeneous film.

The mechanical properties exhibited a clear concentration-dependent trend (Fig. 2C). The tensile strength (TS) progressively declined from 1.85 ± 0.04 MPa (ASA0) to 1.47 ± 0.07 MPa (ASA5), 1.14 ± 0.03 MPa (ASA7), 0.98 ± 0.02 MPa (ASA10), and finally 0.62 ± 0.02 MPa (ASA12). This systematic decrease indicates that high anthocyanin loading disrupts the native Alg/SS intermolecular network, leading to reduced cohesion within the matrix. Similarly, the elongation at break (EAB) decreased from $31.89 \pm 1.26\%$ (ASA0) to $15.56 \pm 0.19\%$ (ASA7) and $13.56 \pm 0.69\%$ (ASA12), reflecting diminished flexibility. At low anthocyanin concentrations, polyphenolic groups can participate in hydrogen-bond-mediated secondary cross-linking, temporarily reinforcing the Alg/SS network. However, as the anthocyanin content increases, these molecules increasingly behave as rigid micro-fillers inserted within the polymer matrix. Their bulky aromatic structures restrict polymer-chain mobility and generate microphase heterogeneity, which interrupts continuous polymer–polymer bonding. This transition from cooperative cross-linking (low anthocyanin) to matrix over-filling and structural discontinuity (high anthocyanin) explains the observed decline in TS and EAB. Therefore, optimizing anthocyanin content is essential to balance mechanical integrity and water resistance for packaging and colorimetric-sensor applications. The full stress–strain curves from the tensile tests are provided in SI S1.

The wettability of the films was evaluated through water contact angle measurements, as shown in Fig. 2D1–D5. The measured contact angles (θ) for ASA0, ASA5, ASA7, ASA10, and ASA12 were 99°, 55.6°, 47°, 38.5°, and 37.2°, respectively. These results indicate that the ASA0 film exhibited the highest hydrophobicity, while the incorporation of anthocyanin extract progressively increased the films' hydrophilicity. This observation is consistent with the previously discussed water solubility results, confirming that anthocyanin addition enhances the affinity of film for water. Moreover, this trend agrees well with previous studies,[42–44] which also reported that anthocyanin or polyphenol incorporation increases the hydrophilic nature of polysaccharide-based films due to the introduction of polar hydroxyl and carboxyl groups capable of forming hydrogen bonds with water molecules.

The surface morphology of the films was examined by SEM images (Fig. 2E1–E5), revealing notable differences between ASA0 and ASA films. ASA0 displayed a uniform surface, likely

due to the sericin incorporated into the alginate matrix and formed uniform structures.[45] In ASA films, the surface was rough and uneven, reflecting incomplete dispersion and occasional aggregation of anthocyanins within the matrix. Similar effects of anthocyanin or plant extract incorporation on film roughness have been reported in previous studies.[32,46,47]

These results demonstrate that increasing anthocyanin concentration modifies the internal structure of ASA films by enhancing hydrogen bonding and hydrophilicity while reducing network uniformity and mechanical cohesion. Considering both the colorimetric responsiveness and the physical characteristics of the films at different anthocyanin levels, the ASA7 film exhibited the most balanced performance. It provided sufficient color intensity and stability while maintaining desirable mechanical integrity, barrier efficiency, and moderate hydrophilicity, which are essential for practical handling and sensing performance. Therefore, the ASA7 formulation is identified as the optimal candidate for subsequent physicochemical characterization and application studies, particularly in the development of pH-responsive smart sensors for real-time freshness monitoring of food products.

3.3. Structural, thermal, and optical properties of ASA films

FTIR spectroscopy was employed to elucidate the molecular interactions within the ASA composite films in comparison with their individual components (Fig. 5A). The ASA0 film displayed spectral features more closely resembling those of sericin rather than alginate[48] and confirming the successful formation of a polysaccharide–protein composite network. Both ASA0 and ASA7 films exhibited characteristic absorption bands corresponding to their major functional groups, indicating that the incorporation of anthocyanins did not introduce new chemical functionalities but instead altered the intermolecular interactions within the matrix. A broad and intensified band in the 3500–3200 cm^{-1} region, assigned to O–H stretching, was markedly stronger in anthocyanin-containing films, suggesting an increased extent of hydrogen bonding among hydroxyl-bearing groups of alginate, sericin, glycerol, and anthocyanins. The amide I (1641–1646 cm^{-1}) and amide II (1530–1535 cm^{-1}) bands associated with the β-sheet structure of SS showed slight intensity variations upon anthocyanin incorporation, which may arise from interactions between anthocyanin aromatic rings and peptide backbones, as well as the C=C stretching of the flavonoid skeleton.[49,50] Additional peaks at 2934–2936 cm^{-1} (C–H stretching) and 1240–1022 cm^{-1} (C–O–C vibrations) were present in all films, although minor shifts were observed in the ASA7 sample, reflecting subtle modifications in the polymer environment. Collectively, these spectral changes indicate the formation of enhanced hydrogen bonding and possible π–π or dipole–dipole interactions between anthocyanins and the Alg/SS matrix. Thus, FTIR analysis confirms that anthocyanin incorporation reinforces intermolecular interactions and improves interfacial compatibility within the polymer network without altering its fundamental chemical structure.

The thermal behavior of the composites and their individual constituents was evaluated using TGA and DSC under an air atmosphere at a heating rate of 10 °C min^{-1} (Fig. 3B and C). As shown in Fig. 3B, the TGA profile of the ASA0 film differs markedly from those of pure Alg and SS, confirming the formation of new composite structures. For the ASA0 film, an initial mass loss observed between 50 and 110 °C corresponds to the evaporation of physically adsorbed water. A major

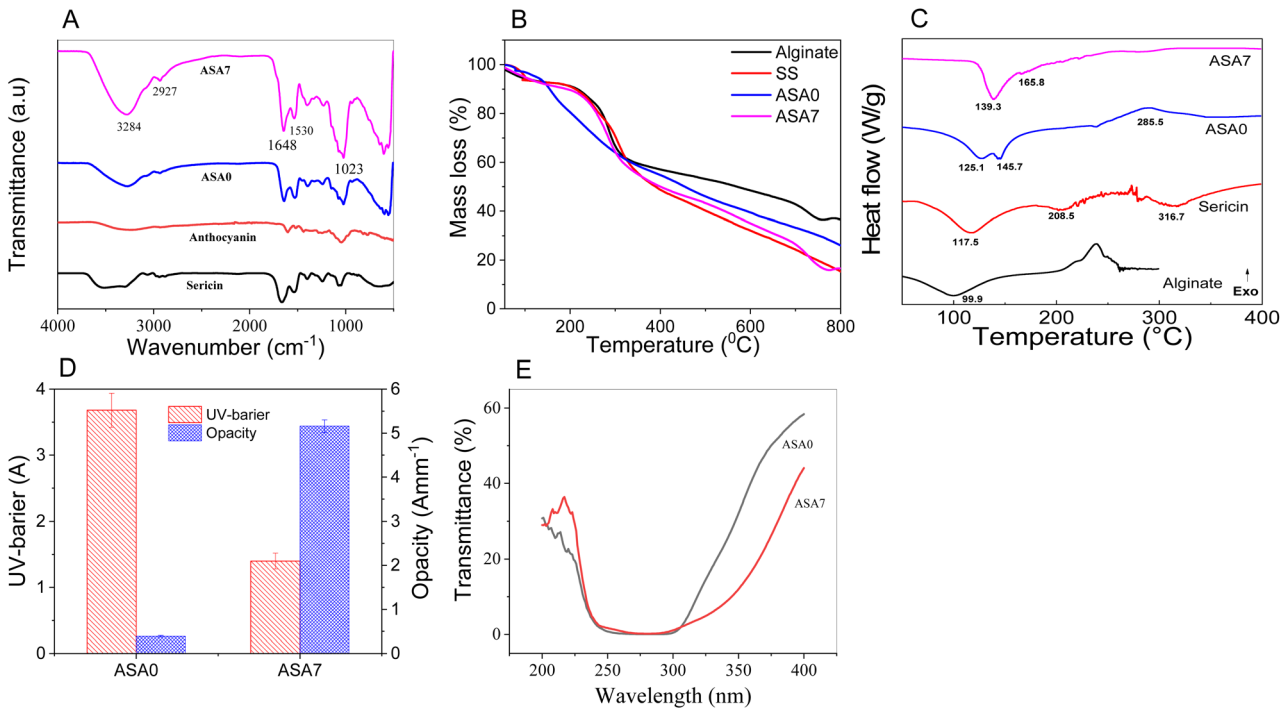

Fig. 3 IR spectra (A), TGA curves (B), DSC curves (C) and UV barrier (D and E) of components, and ASA0 and ASA7 films.

decomposition event occurs up to 800 °C, resulting in an overall mass loss of approximately 61%. The divergence in thermal behavior between ASA0 and its components reflects the molecular interactions between polysaccharide and protein chains within the composite matrix.

In contrast, the ASA7 film undergoes a three-stage thermal degradation process from 50 to 800 °C. The first stage (50–200 °C) accounts for about 10% mass loss, primarily associated with moisture release and degradation of low-molecular-weight species. The second stage (200–300 °C) contributes approximately 40% mass loss, corresponding to the breakdown of the polymer backbone. The final stage (300–800 °C) leads to an additional 35% mass reduction, attributable to further degradation and carbonization. The higher overall mass loss of ASA7 compared with ASA0 is linked to the presence of anthocyanins, which alter the composite network and influence its thermal decomposition pathways. Despite its multistep degradation profile, the ASA7 film exhibits improved thermal stability, indicating that anthocyanin incorporation enhances structural integrity at elevated temperatures.

DSC curves were obtained to elucidate the thermal transitions of the prepared films. The alginate film exhibited a single low-temperature endothermic event at 99.9 °C, attributable to bound-water evaporation or the glass transition, confirming its predominantly amorphous structure and lack of crystalline domains. In contrast, sericin films displayed a clear T_g at 117.5 °C and a broader peak at 208.5 °C, followed by decomposition near 316.7 °C, attributed to protein carbonization and degradation of SS.[51] Notably, the ASA0 composite film presented an intermediate thermal profile, with T_g values of 125.1 °C and 145.7 °C, higher than that of its components. This shift suggests the formation of intermolecular interactions, particularly hydrogen bonding, between sericin and alginate chains, leading to a more integrated polymer network with enhanced structural stability. Upon incorporation of anthocyanins, the ASA film exhibited T_g values of 139.3 °C and 165.8 °C, indicating improved thermal stability likely arising from strong interactions between the pigment molecules and the Alg/SS matrix.[52] The introduction of anthocyanins and the resulting reinforcement of polymer–polyphenol interactions contributed to increased T_g values, consistent with the improved mechanical strength and heat resistance observed in the composite films. These DSC results collectively demonstrate that the developed films possess sufficient thermal robustness for practical use in smart food-packaging applications.

Light exposure is one of the primary drivers of oxidative degradation in food systems; consequently, packaging materials with strong UV-blocking capacity are crucial for maintaining color stability. In addition, visible-light transmittance data provide insights into the homogeneity of polymer blends, thereby enabling assessment of sample uniformity.[29] As illustrated in Fig. 3C and D, the incorporation of anthocyanins markedly decreased visible-light transmittance compared to that of the ASA0 film. The ASA7 film, in particular, exhibited substantially improved UV-shielding behavior, highlighting its potential to protect food products from photodegradation. This enhancement in light-barrier performance is largely attributed to the intrinsic UV-absorbing properties of phenolic chromophores, which strongly absorb in both the UV-A and portions of the visible region.[24] Consistently, the ASA7 film displayed a significantly higher opacity value (5.16 ± 0.15 A mm^{-1}) relative to the ASA0 film (0.39 ± 0.02 A mm^{-1}), confirming its reduced transparency. The lower transmittance and higher opacity result from anthocyanin pigments absorbing light predominantly in the yellow-green region, thereby limiting light penetration through the film.[53]

Together, the FTIR, TGA, DSC, and UV-vis results demonstrate that anthocyanin incorporation reinforces intermolecular interactions, thereby improving the homogeneity of the polymer blend while simultaneously enhancing thermal stability and UV-shielding performance of the Alg/SS matrix. These synergistic effects ultimately produce a more robust and functional smart packaging material suitable for real-time freshness monitoring.

3.4. Antioxidant activity of ASA biofilms

Antioxidant activity plays a dual role in food systems, as it can both delay oxidation and contribute to spoilage, potentially posing dietary health risks. Environmental factors such as light, humidity, and temperature significantly influence food quality. The incorporation of antioxidants into packaging films has been shown to enhance their ability to preserve the nutritional value, quality, and safety of food products.[33] The antioxidant capacity of the anthocyanin-enriched film ASA7 was evaluated using two methods. The DPPH RSA of the ASA7 sample ($37.10 \pm 1.71\%$) was higher than that of the Alg/SS sample ($33.56 \pm 0.97\%$). Similarly, the ASA7 sample exhibited stronger HPS ($90.37 \pm 1.30\%$) compared to the Alg/SS sample ($76.12 \pm 2.01\%$), reflecting the enhanced capacity of the film to neutralize hydrogen peroxide and inhibit oxidative stress. This assay is based on the formation of the orange Fe^{2+}-1,10-phenanthroline complex, which is inhibited by H_2O_2. The ASA7 biofilm restores complex formation, indicating effective H_2O_2 neutralization. Both anthocyanins and sericin can provide additional hydrogen-donating groups, and contribute synergistically to the antioxidant activity. The polyphenolic anthocyanins extracted from mangosteen peel are well-known for their strong radical-scavenging ability, while SS present in the film contributes to the antioxidant effect through its amino acid residues, such as serine and threonine, which can interact with reactive species.[26,54,55] These results highlight the enhanced oxidative stability of the ASA film, supporting their potential application as active materials for food packaging aimed at protecting against oxidative spoilage.

3.5. Sustainability & carbon footprint

Although a full life cycle assessment was not performed, the production of the films is anticipated to have a relatively low environmental impact. The films are fabricated using renewable, biobased materials, including SS, alginate, and anthocyanin, which are naturally abundant or derived from food waste. The fabrication process involves mild processing conditions with minimal use of hazardous chemicals, reducing energy

consumption and greenhouse gas emissions compared to conventional petroleum-based polymers. Given the growing concerns over plastic pollution and greenhouse gas emissions, developing films from renewable and waste-derived biopolymers represents a promising strategy to mitigate environmental impact while maintaining functional performance. This approach aligns with current strategies for sustainable, low-carbon biopolymer materials reported in the literature.[56–59] Moreover, utilizing biobased precursors and energy-efficient processes enhances the eco-friendliness of the films and supports principles of circular economy, highlighting their potential as environmentally responsible alternatives for packaging applications. Therefore, the developed fabrication pathway offers not only functional film performance but also contributes to lowering the carbon-related burden of packaging materials, making it more compatible with current sustainability-driven expectations in food-contact applications.

3.6. Monitoring freshness of ASA biofilms

3.6.1. Shrimp freshness. In protein-rich foods such as seafood and meat, microbial decomposition and enzymatic hydrolysis of proteins generate volatile nitrogenous compounds, primarily ammonia (NH_3), trimethylamine (TMA), and dimethylamine (DMA), which gradually accumulate during storage. These basic compounds elevate the pH of the surrounding environment, producing an alkaline microclimate at the film-food interface. The consequent pH shifts trigger visible color transitions in pH-sensitive films, providing a non-destructive means to monitor freshness in real time. Such colorimetric polysaccharide-based indicator films have been widely investigated for freshness evaluation in shrimp and other perishable seafoods.[60] The TVB-N content serves as a recognized quantitative index of seafood spoilage. According to standard classification criteria, shrimp are considered fresh when TVB-N is below 12 mg N/100 g, partially decomposed between 12 and 25 mg N/100 g, and spoiled when exceeding 25 mg N/100 g.[21]

To evaluate the colorimetric performance of the ASA films, shrimp samples were stored at room temperature for 14 hours, with both films ASA7 and ASA12. TVB-N contents were monitored at defined intervals (Fig. 4A and B). During the first 4 hours, the ASA films retained their initial pink hue, while the TVB-N value increased slightly to 13.41 ± 0.55 mg N/100 g, indicating early-stage freshness deterioration yet remaining within acceptable limits. As storage continued for 8 and 10 hours, the TVB-N levels increased to 20.55 ± 0.18 mg N/100 g and 25.08 ± 0.15 mg N/100 g, respectively, corresponding to the transition toward the critical spoilage threshold. At these time points, both films exhibited a distinct color transition from pink to violet, indicating the onset of protein degradation and the release of volatile amines. However, the ASA7 film showed a more pronounced and easily distinguishable color change to the naked eye compared with the ASA12 film, suggesting superior visual sensitivity for detecting the initial stages of spoilage. After 14 hours of storage, the TVB-N content reached 38.12 mg N/100 g, surpassing the spoilage threshold and confirming advanced shrimp decomposition. The results indicated that ASA films possess the potential for real-time colorimetric detection of TVB-N content in food samples.

For detection of RGB ratios using a smartphone (Fig. 4C and D), both ASA7 and ASA12 films exhibited a comparable colorimetric response pattern during shrimp storage, showing a gradual transition from pinkish-red to bluish-violet as protein degradation progressed. As the TVB-N values increased from

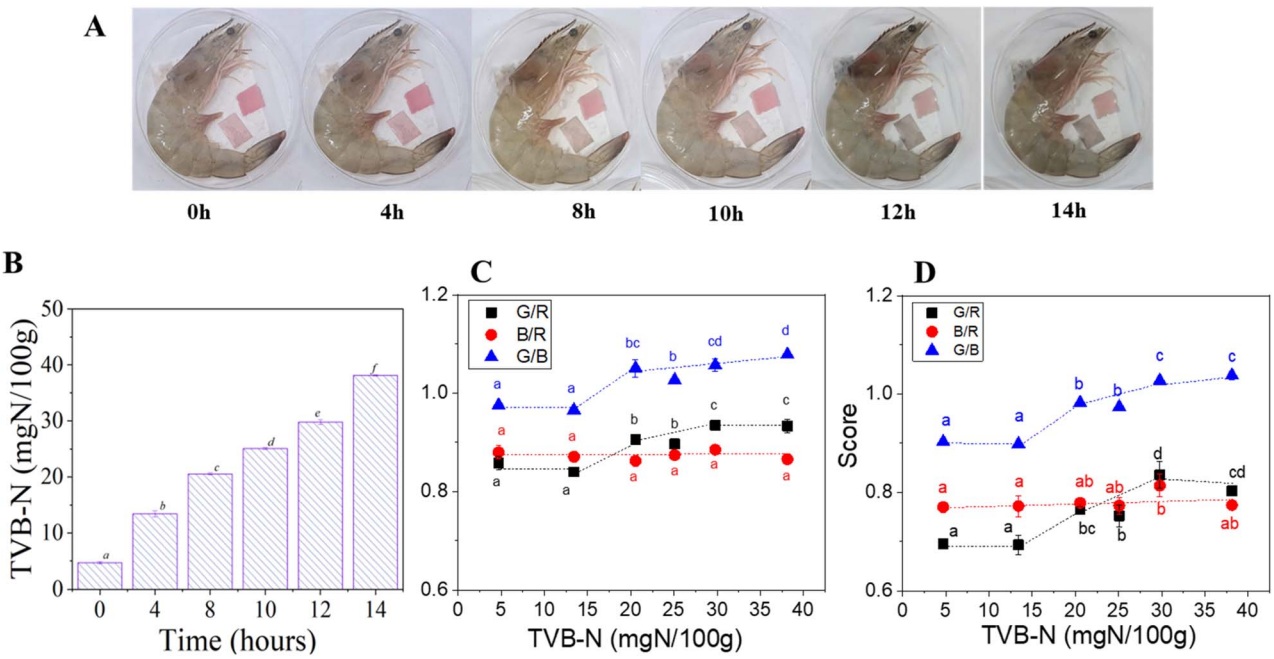

Fig. 4 The images of shrimp and indicator films ASA7 and ASA12 (A), plots of TVB-N *versus* storage time (B) after 14 h at room temperature and plots of RGB ratios of ASA7 (C) and ASA12 (D). Different letters showed significant differences ($p < 0.05$).

4.69 ± 0.21 to 38.12 ± 0.41 mg N/100 g, both films displayed measurable shifts in chromatic parameters, reflecting their responsiveness to spoilage-induced pH variation. For ASA12, the green/red ratio increased modestly from 0.69 ± 0.01 to 0.80 ± 0.01, while green/blue increased from 0.90 ± 0.00 to 1.04 ± 0.01, indicating a consistent though moderate color evolution. In comparison, ASA7 exhibited a slightly more pronounced progression, with red/green increasing from 0.86 ± 0.01 to 0.93 ± 0.01 and green/blue from 0.97 ± 0.00 to 1.08 ± 0.01, producing a clearer visual contrast observable by the naked eye. At 8 h of storage, when TVB-N reached 20.55 ± 0.18 mg N/100 g, a level just below the seafood spoilage limit of 25 mg N/100 g, both films already exhibited noticeable color deviation, signifying the onset of spoilage detection prior to the critical threshold. This early visual response is attributed to the generation of volatile amines, which increase the local pH at the film-food interface, triggering anthocyanin structural transformation from the red flavylium form to quinoidal and chalcone species that yield bluish-violet hues. Generally, both ASA7 and ASA12 demonstrated reliable colorimetric responses to spoilage; however, ASA7 achieved higher visual clarity and earlier detection, confirming its suitability as the optimized formulation for practical freshness monitoring.

The strong correlation between RGB values and TVB-N confirms that the anthocyanin-based film functions not merely as a qualitative color tag but as a predictive freshness indicator. Notably, the film exhibited a visible inflection point (pale pink → whitish) before TVB-N approached the regulatory rejection limit, demonstrating an effective early-warning and real-time response. This behavior is consistent with spoilage-responsive films reported in the literature, though the magnitude of color change observed here is more pronounced. For instance, Choubaki *et al.* (2025) documented only a modest ΔE shift in pomegranate-flower anthocyanin films applied to trout, with visible changes emerging after microbial counts exceeded acceptable limits.[6] Similarly, Zeng *et al.* (2023) showed that pectin–chitosan films containing black-rice anthocyanins transitioned from red to blue during meat deterioration, confirming their sensitivity to spoilage.[61] Kwak *et al.* (2024) also reported a strong relationship between TVB-N and color evolution in GA/gelatin/anthocyanin/PVA films, where indicator color shifted from purple (9.8 ± 0.2 mg N/100 g) to purple-blue (21.0 ± 2.5 mg N/100 g) and finally to blue at 34 h (37.1 ± 0.5 mg N/100 g).[62] These comparisons highlight that the present film provides a sharper and earlier visual response than many existing anthocyanin-based indicators, enhancing its suitability for real-time freshness monitoring.

3.6.2. Pork meat freshness. The colorimetric sensing performance of the ASA7 biofilm toward pork freshness monitoring was evaluated by tracking time-dependent color variations during 24 hours of storage at room temperature (Fig. 5A and B). Throughout the storage period, the pork samples exhibited a gradual loss of freshness, as evidenced by the visible fading of meat color from bright red to brownish-gray, a typical indicator of myoglobin oxidation and protein decomposition. This visual degradation correlated well with the progressive increase in TVB-N, which increased from 5.05 ± 0.08 mg N/100 g at the initial stage to 36.67 ± 0.14 mg N/100 g after 24 h, confirming the accumulation of volatile amines resulting from enzymatic and microbial proteolysis under ambient conditions. The ASA7 indicator film showed a relatively moderate but consistent color response to these biochemical changes. During

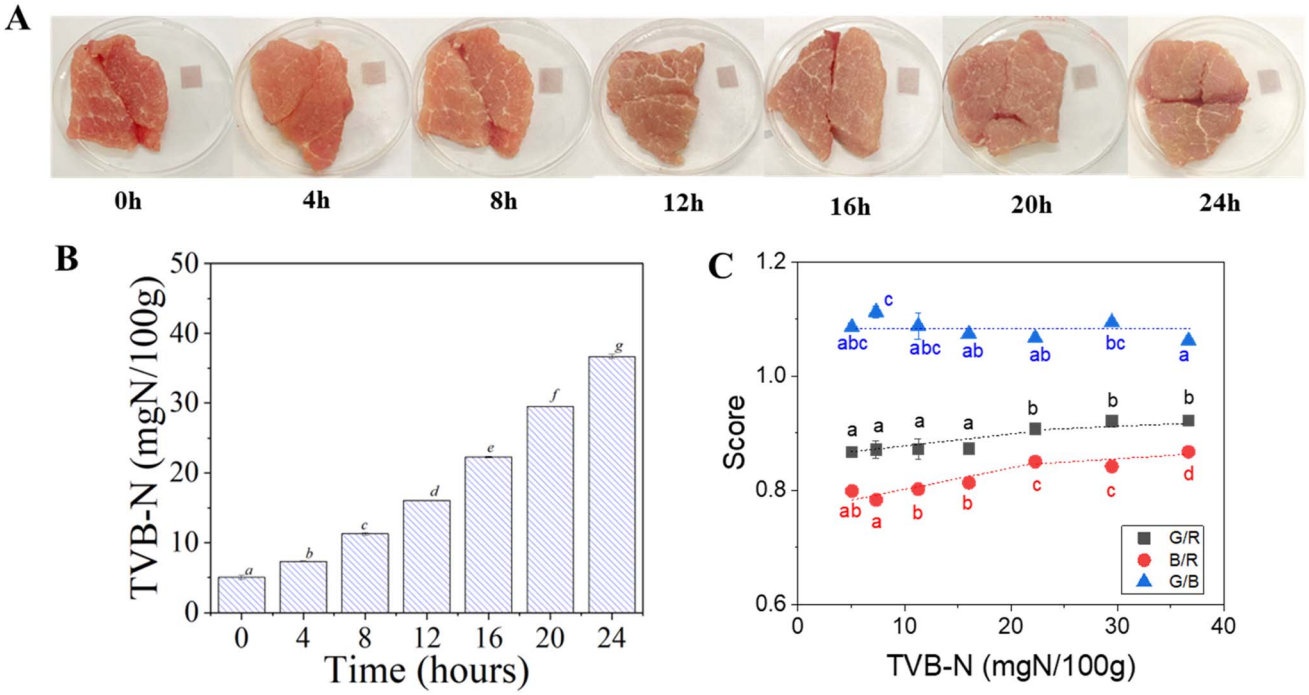

Fig. 5 The images of shrimp and indicator film ASA7 (A), plots of TVB-N *versus* storage time of 24 h at room temperature (B) and plots of RGB ratios of ASA7 (C). Different letters showed significant differences ($p < 0.05$).

the first 16 hours, the film largely retained its reddish-pink hue, with only slight fading observable when the TVB-N value reached 22.27 ± 0.07 mg N/100 g, still below the general spoilage threshold (25 mg N/100 g). By the end of storage (24 h), a perceptible shift toward a pale violet tone emerged, reflecting the onset of advanced degradation, although the overall color transition remained weaker than that observed in shrimp samples.

As shown in Fig. 5C, quantitative color analysis revealed moderate variations in RGB ratios. The red/blue ratio increased from 0.799 to 0.850 after 16 h ($p < 0.05$), indicating partial oxidation and pigment transformation within the film matrix. The green/blue ratio displayed a non-linear trend—peaking at 1.112 after 4 h and slightly decreasing to 1.062 after 24 h, suggesting dynamic interactions between the released amines and the embedded anthocyanin. However, the magnitude of these colorimetric shifts was smaller than those recorded for shrimp, which can be attributed to the slower decomposition kinetics of pork.[63] The reduced rate of amine release likely limits gas diffusion and pH elevation near the film surface, thereby delaying anthocyanin structural conversion from the flavylium form to its quinoidal and chalcone derivatives. Therefore, the ASA film exhibited lower visual contrast and slower response toward meat spoilage compared with seafood, and it still demonstrated clear qualitative sensing ability. These findings highlight the film's potential applicability as a biodegradable freshness indicator, particularly suitable for rapidly perishable foods such as shrimp, where decomposition is faster and colorimetric detection is more pronounced.

4 Conclusion

This study reports the development of a biodegradable, pH-responsive ASA film composed of alginate, sericin, and mangosteen-peel anthocyanins, capable of visually indicating freshness deterioration in protein-rich foods. In addition to the strong correlation established between chromatic transitions and biochemical spoilage markers, the findings underscore the broader potential of valorizing agro-industrial residues by transforming sericin waste and fruit-peel byproducts into high-value functional materials. The film's rapid and sensitive response to foodborne metabolic changes demonstrates its relevance for consumer safety, offering an accessible, non-instrumental means of detecting early stages of product degradation. Moving forward, future work should emphasize validating the system under realistic commercial conditions, including cold-chain storage, sealed packaging formats, and extended shelf-life scenarios across diverse food matrices. Such investigations will enhance the film's technological readiness and accelerate its integration into large-scale intelligent packaging solutions that advance both food safety management and sustainable waste-reduction strategies.

Author contributions

Thi-Hong-No Nguyen: investigation, formal analysis, validation, software, originate manuscript; Minh-Truong Truong, Minh-Ty Nguyen, Quynh-Nhu Pham, Dinh-Tri Mai, Thi-Quynh-Nhu Ngo, Thi-Ngoc-Mai Tran, Ngoc-Bich-Tuyen Nguyen, Chi-Hien Dang, Huu-Trung Nguyen and Cao-Hien Nguyen: investigation, visualization, validation; Thanh-Danh Nguyen: conceptualization, supervision, writing – review & editing.

Conflicts of interest

The authors of this paper state that they have no competing financial interests or personal relationships that could have influenced the reported work.

Data availability

The data supporting this article have been included as part of the supplementary information (SI). Supplementary information is available. See DOI: https://doi.org/10.1039/d5fb00753d.

Acknowledgements

This research was funded by the Vietnam Academy of Science and Technology under grant number NCXS02.04/24–25.

References

1 M. Ghaani, C. A. Cozzolino, G. Castelli and S. Farris, An overview of the intelligent packaging technologies in the food sector, *Trends Food Sci. Technol.*, 2016, **51**, 1–11.
2 H. Cheng, H. Xu, D. J. McClements, L. Chen, A. Jiao, Y. Tian, M. Miao and Z. Jin, Recent advances in intelligent food packaging materials: Principles, preparation and applications, *Food Chem.*, 2022, **375**, 131738.
3 Janseerat, M. Kolekar, C. S. Reddy, S. Sharma and S. Roy, Anthocyanin-based natural color induced intelligent food packaging sensor: A review, *Curr. Food Sci. Technol. Rep.*, 2024, **2**(2), 157–167.
4 S. Singh, K. K. Gaikwad and Y. S. Lee, Anthocyanin-A natural dye for smart food packaging systems, *Korean J. Packag. Sci. Technol.*, 2018, **24**(3), 167–180.
5 S. Shiryanpour, L. Nouri, M. Azizi, A. Najafi and A. Mohammadi Nafchi, Active chitosan film containing single and double nanoemulsions of Oliveira decumbens Vent essential oil/anthocyanin of eggplant for chicken preservation: S. Shiryanpour et al, *J. Food Meas. Char.*, 2025, **19**(10), 7381–7403.
6 S. Choubaki, H. Baghaei and A. Mohammadi Nafchi, Smart Indicator for Fish Freshness Monitoring: A Chitosan/Gelatin/Zinc Oxide Nanoparticle Composite Incorporating Pomegranate Flower Anthocyanin Extract Nanocapsules, *Food Sci. Nutr.*, 2025, **13**(9), e70944.
7 X. Chen, H. Xiang, Y. Liang, J. He, R. Chen, Z. Zhu, S. Li, X. Chen and S. Cheng, Highly stable and multifunctional intelligent film based on grape skin anthocyanin, polyvinyl alcohol, chitosan and selenopeptide: Preparation, characterization and application, *Food Hydrocoll.*, 2025, **158**, 110546.
8 S. Gomez, B. Pathrose, M. Joseph, M. Shynu and B. Kuruvila, Comparison of extraction methods on anthocyanin pigment

attributes from mangosteen (Garcinia mangostana L.) fruit rind as potential food colourant, *Food Chem. Adv.*, 2024, **4**, 100559.
9 R. Aad, I. Dragojlov and S. Vesentini, Sericin protein: structure, properties, and applications, *J. Funct. Biomater.*, 2024, **15**(11), 322.
10 A. S. Silva, E. C. Costa, S. Reis, C. Spencer, R. C. Calhelha, S. P. Miguel, M. P. Ribeiro, L. Barros, J. A. Vaz and P. Coutinho, Silk sericin: a promising sustainable biomaterial for biomedical and pharmaceutical applications, *Polymers*, 2022, **14**(22), 4931.
11 D. Vurro, A. Liboà, I. D'Onofrio, G. De Giorgio, Z. Zhou, V. Galstyan, Y. Qin, X. Huang, P. D'Angelo and G. Tarabella, Recycled Sericin Biopolymer in Biotechnology and Bioelectronics, *Bioengineering*, 2025, **12**(5), 547.
12 G. T. Hailu, M. T. Alemea and F. Lemessa, Development of silk sericin-based polysaccharide-protein hybrid biofilms: Mechanical, thermal, and antibacterial properties, *Next Res.*, 2025, **2**(1), 100097.
13 S. J. Seo, K.-J. Im, H.-S. Shin, G. Das and J. K. Patra, Application of Sericin-Based Materials in Food Packaging: An Overview, *Biol. Life Sci. Forum.*, 2021, **6**, 40.
14 S. Kumar, S. Biswas, P. K. Byram, P. V. Vaidya, S. Dhara, N. Chakravorty and M. Kaushal, Sericin and Xanthan gum-based biopolymer films with enhanced stretchability and cell-proliferation capability, *Carbohydr. Polym.*, 2025, 123675.
15 T. Senturk Parreidt, K. Müller and M. Schmid, Alginate-based edible films and coatings for food packaging applications, *Foods*, 2018, **7**(10), 170.
16 N. Abdullah, Z. Mohamad, Z. I. Khan, M. Jusoh, Z. Y. Zakaria and N. Ngadi, Alginate based sustainable films and composites for packaging: A review, *Chem. Eng.*, 2021, **83**, 271–276.
17 K. Y. Lee and D. J. Mooney, Alginate: properties and biomedical applications, *Prog. Polym. Sci.*, 2012, **37**(1), 106–126.
18 H. E. Tahir, S. B. Hashim, G. K. Mahunu, M. Arslan, S. Jiyong, A. A. Mariod, J. Zhang, H. R. El-Seedi, X. Zhai and T. H. Musa, Smart films fabricated from natural pigments for measurement of total volatile basic nitrogen (TVB-N) content of meat for freshness evaluation: A systematic review, *Food Chem.*, 2022, **396**, 133674.
19 M. Zam, I. Niyumsut, K. Osako and S. Rawdkuen, Fabrication and characterization of intelligent multi-layered biopolymer film incorporated with pH-sensitive red cabbage extract to indicate fish freshness, *Polymers*, 2022, **14**(22), 4914.
20 H.-z. Chen, M. Zhang, B. Bhandari and C.-h. Yang, Novel pH-sensitive films containing curcumin and anthocyanins to monitor fish freshness, *Food Hydrocoll.*, 2020, **100**, 105438.
21 H. Dong, Z. Ling, X. Zhang, X. Zhang, S. Ramaswamy and F. Xu, Smart colorimetric sensing films with high mechanical strength and hydrophobic properties for visual monitoring of shrimp and pork freshness, *Sens. Actuators, B*, 2020, **309**, 127752.
22 J. Yan, R. Cui, Y. Qin, L. Li and M. Yuan, A pH indicator film based on chitosan and butterfly pudding extract for monitoring fish freshness, *Int. J. Biol. Macromol.*, 2021, **177**, 328–336.
23 Y. Qin, Y. Wang, Z. Tang, K. Chen, Z. Wang, G. Cheng, H. Chi and T. Soteyome, A pH-sensitive film based on chitosan/gelatin and anthocyanin from Zingiber striolatum Diels for monitoring fish freshness, *Food Chem.: X*, 2024, **23**, 101639.
24 X. Wang, H. Yong, L. Gao, L. Li, M. Jin and J. Liu, Preparation and characterization of antioxidant and pH-sensitive films based on chitosan and black soybean seed coat extract, *Food Hydrocoll.*, 2019, **89**, 56–66.
25 T.-H.-N. Nguyen, V.-K.-D. Nguyen, M.-V. Phan, Q.-N. Pham, M.-H. Do, T.-Q. Le, M.-T. Nguyen and T.-D. Nguyen, A facile fabrication method of sericin/chitosan film without additives for fruit coating, *RSC Adv.*, 2025, **15**(25), 19704–19713.
26 L. Hiranrangsee, K. K. Kumaree, M. B. Sadiq and A. K. Anal, Extraction of anthocyanins from pericarp and lipids from seeds of mangosteen (Garcinia mangostana L.) by Ultrasound-assisted extraction (UAE) and evaluation of pericarp extract enriched functional ice-cream, *J. Food Sci. Technol.*, 2016, **53**(10), 3806–3813.
27 T. T. T. Nguyen, T. Q. Le, T. T. A. Nguyen, L. T. M. Nguyen, D. T. C. Nguyen and T. Van Tran, Characterizations and antibacterial activities of passion fruit peel pectin/chitosan composite films incorporated Piper betle L. leaf extract for preservation of purple eggplants, *Heliyon*, 2022, **8**(8), e10096.
28 K. Zhang, T.-S. Huang, H. Yan, X. Hu and T. Ren, Novel pH-sensitive films based on starch/polyvinyl alcohol and food anthocyanins as a visual indicator of shrimp deterioration, *Int. J. Biol. Macromol.*, 2020, **145**, 768–776.
29 H. Yong, X. Wang, R. Bai, Z. Miao, X. Zhang and J. Liu, Development of antioxidant and intelligent pH-sensing packaging films by incorporating purple-fleshed sweet potato extract into chitosan matrix, *Food Hydrocoll.*, 2019, **90**, 216–224.
30 P. Ezati and J.-W. Rhim, pH-responsive pectin-based multifunctional films incorporated with curcumin and sulfur nanoparticles, *Carbohydr. Polym.*, 2020, **230**, 115638.
31 X. Pan, G. Chen, T. Xu, L. Kong, X. Li, D. Li, C. Mu, Z. Xu and L. Ge, Gelatin-based active edible film with pH-sensing for maintaining and monitoring fish freshness, *ACS Food Sci. Technol.*, 2023, **3**(8), 1366–1375.
32 N. H. Che Hamzah, N. Khairuddin, I. I. Muhamad, M. A. Hassan, Z. Ngaini and S. R. Sarbini, Characterisation and colour response of smart sago starch-based packaging films incorporated with Brassica oleracea anthocyanin, *Membranes*, 2022, **12**(10), 913.
33 Y.-T. Kim, R. Kimmel and X. Wang, A New Method to Determine Antioxidant Activities of Biofilms Using a pH Indicator (Resazurin) Model System, *Molecules*, 2023, **28**(5), 2092.
34 D. Mukhopadhyay, P. Dasgupta, D. S. Roy, S. Palchoudhuri, I. Chatterjee, S. Ali and S. G. Dastidar, A sensitive in vitro spectrophotometric hydrogen peroxide scavenging assay

using 1, 10-phenanthroline, *Free Radic. Antioxid.*, 2016, **6**(1), 124–132.

35 N. P. S. Velho, Preparation for obtaining accreditation of analytical methods regarding quality issues as stated in ISO standard ISO/IEC 17025: 1999, *Final Project Report*, 2001.

36 H. Ayvaz, T. Cabaroglu, A. Akyildiz, C. U. Pala, R. Temizkan, E. Ağçam, Z. Ayvaz, A. Durazzo, M. Lucarini and R. Direito, Anthocyanins: Metabolic digestion, bioavailability, therapeutic effects, current pharmaceutical/industrial use, and innovation potential, *Antioxidants*, 2022, **12**(1), 48.

37 G. C. Vidana Gamage, Y. Y. Lim and W. S. Choo, Anthocyanins from Clitoria ternatea flower: Biosynthesis, extraction, stability, antioxidant activity, and applications, *Front. Plant Sci.*, 2021, **12**, 792303.

38 D. Yun, H. Cai, Y. Liu, L. Xiao, J. Song and J. Liu, Development of active and intelligent films based on cassava starch and Chinese bayberry (Myrica rubra Sieb. et Zucc.) anthocyanins, *RSC Adv.*, 2019, **9**(53), 30905–30916.

39 L. G. Santos, G. F. Alves-Silva and V. G. Martins, Active-intelligent and biodegradable sodium alginate films loaded with Clitoria ternatea anthocyanin-rich extract to preserve and monitor food freshness, *Int. J. Biol. Macromol.*, 2022, **220**, 866–877.

40 S. Mohammadalinejhad, M. Kurek, I.-J. Jensen and J. Lerfall, The potential of anthocyanin-loaded alginate hydrogel beads for intelligent packaging applications: Stability and sensitivity to volatile amines, *Curr. Res. Food Sci.*, 2023, **7**, 100560.

41 C. Torres-León, A. A. Vicente, M. L. Flores-López, R. Rojas, L. Serna-Cock, O. B. Alvarez-Pérez and C. N. Aguilar, Edible films and coatings based on mango (var. Ataulfo) by-products to improve gas transfer rate of peach, *LWT-Food Sci. Technol.*, 2018, **97**, 624–631.

42 L. Zhao, Y. Liu, L. Zhao and Y. Wang, Anthocyanin-based pH-sensitive smart packaging films for monitoring food freshness, *J. Agric. Food Res.*, 2022, **9**, 100340.

43 R. Abedi-Firoozjah, S. Yousefi, M. Heydari, F. Seyedfatehi, S. Jafarzadeh, R. Mohammadi, M. Rouhi and F. Garavand, Application of red cabbage anthocyanins as pH-sensitive pigments in smart food packaging and sensors, *Polymers*, 2022, **14**(8), 1629.

44 L. N. Remedio and C. Parada Quinayá, Intelligent packaging systems with anthocyanin: Influence of different polymers and storage conditions, *Polymers*, 2024, **16**(20), 2886.

45 J. G. de Oliveira Filho, J. M. Rodrigues, A. C. F. Valadares, A. B. de Almeida, T. M. de Lima, K. P. Takeuchi, C. C. F. Alves, H. A. de Figueiredo Sousa, E. R. da Silva and F. H. Dyszy, Active food packaging: Alginate films with cottonseed protein hydrolysates, *Food Hydrocoll.*, 2019, **92**, 267–275.

46 L. M. Coelho, C. Faria, D. Madalena, Z. Genisheva, J. T. Martins, A. A. Vicente and A. C. Pinheiro, Valorization of amaranth (Amaranthus cruentus) grain extracts for the development of alginate-based active films, *Molecules*, 2022, **27**(18), 5798.

47 C. L. Luchese, N. Sperotto, J. C. Spada and I. C. Tessaro, Effect of blueberry agro-industrial waste addition to corn starch-based films for the production of a pH-indicator film, *Int. J. Biol. Macromol.*, 2017, **104**, 11–18.

48 T.-D. Nguyen, C.-H. Dang and D.-T. Mai, Biosynthesized AgNP capped on novel nanocomposite 2-hydroxypropyl-β-cyclodextrin/alginate as a catalyst for degradation of pollutants, *Carbohydr. Polym.*, 2018, **197**, 29–37.

49 X. Zhang and P. Wyeth, Using FTIR spectroscopy to detect sericin on historic silk, *Sci. China Chem.*, 2010, **53**(3), 626–631.

50 M. Sohany, I. S. M. A. Tawakkal, S. H. Ariffin, N. N. A. K. Shah and Y. A. Yusof, Characterization of anthocyanin associated purple sweet potato starch and peel-based pH indicator films, *Foods*, 2021, **10**(9), 2005.

51 R. A. Priya, P. Roy, R. Sailaja, A. Rangi, T. Sreenivasa and S. V. Naik, Microwave assisted grafting kinetic of alginate/sericin with acrylic acid-co-acrylamide encapsulation of NPK fertilizer and assessment of release characteristics, *Polym. Bull.*, 2024, **81**(13), 1–25.

52 E. D. Freitas, J. M. Vidart, M. G. da Silva and M. G. Vieira, Thermal characterization and stability investigation of sericin and alginate blend loaded with diclofenac sodium or ibuprofen, *Eur. Polym. J.*, 2021, **142**, 110125.

53 S. A. Mir, B. Dar, A. A. Wani and M. A. Shah, Effect of plant extracts on the techno-functional properties of biodegradable packaging films, *Trends Food Sci. Technol.*, 2018, **80**, 141–154.

54 G. Sangwong, M. Sumida and V. Sutthikhum, Antioxidant activity of chemically and enzymatically modified sericin extracted from cocoons of Bombyx mori, *Biocatal. Agric. Biotechnol.*, 2016, **5**, 155–161.

55 W. Widowati, C. N. Ginting, I. N. E. Lister, E. Girsang, A. Amalia, S. H. B. Wibowo and H. S. W. Kusuma, Anti-aging effects of mangosteen peel extract and its phytochemical compounds: Antioxidant activity, enzyme inhibition and molecular docking simulation, *Trop. Life Sci. Res.*, 2020, **31**(3), 127.

56 S. Kim, J. Kim, Y. Kim, J. Yoon, H. Kim, H. Lim, S.-G. Kim, D. Seo, C.-E. Kim and H.-J. Jin, Sustainable bioactive films from sericin and carbon quantum dots: A green approach to smart food packaging, *React. Funct. Polym.*, 2025, 106493.

57 A. B. Kharissova, O. V. Kharissova, B. I. Kharisov and Y. P. Méndez, Carbon negative footprint materials: a review, *Nano-Struct. Nano-Objects*, 2024, **37**, 101100.

58 B. Y. Zhang, Y. Tong, S. Singh, H. Cai and J.-Y. Huang, Assessment of carbon footprint of nano-packaging considering potential food waste reduction due to shelf life extension, *Resour. Conserv. Recycl.*, 2019, **149**, 322–331.

59 M. Zubair, Z. Rauf, H. Nawaz, S. Shahzad and A. Ullah, A review of recent advances in starch derived bionanocomposites for food packaging applications, *Nano-Struct. Nano-Objects*, 2024, **39**, 101204.

60 P. Zeng, X. Chen, Y.-R. Qin, Y.-H. Zhang, X.-P. Wang, J.-Y. Wang, Z.-X. Ning, Q.-J. Ruan and Y.-S. Zhang, Preparation and characterization of a novel colorimetric indicator film based on gelatin/polyvinyl alcohol incorporating mulberry anthocyanin extracts for monitoring fish freshness, *Food Res. Int.*, 2019, **126**, 108604.

61 F. Zeng, Y. Ye, J. Liu and P. Fei, Intelligent pH indicator composite film based on pectin/chitosan incorporated with black rice anthocyanins for meat freshness monitoring, *Food Chem.: X*, 2023, **17**, 100531.
62 M. Kwak and S. C. Min, Monitoring Meat Freshness with Intelligent Colorimetric Labels Containing Red Cabbage Anthocyanins Copigmented with Gelatin and Gallic Acid, *Foods*, 2024, **13**(21), 3464.
63 D. Kossyvaki, M. Contardi, A. Athanassiou and D. Fragouli, Colorimetric indicators based on anthocyanin polymer composites: A review, *Polymers*, 2022, **14**(19), 4129.